Structural Engineering and Mechanics, Vol. 45, No.3 (2013) 337-354

DOI: http://dx.doi.org/10.12989/sem.2013.45.3.337

Full-scale testing and modeling of the mechanical behavior of shield TBM tunnel joints

Wen-qi Ding[1,2,a], Yi-cheng Peng[1,2], Zhi-guo Yan[*1,2], Bi-wei Shen[1,2], He-hua Zhu[1,2,a] and Xin-xin Wei[1,2]

[1]*Department of Geotechnical Engineering, Tongji University, Shanghai, China*
[2]*Key Laboratory of Geotechnical and Underground Engineering of Ministry of Education, Tongji University, Shanghai, China*

(Received June 18, 2012, Revised December 3, 2012, Accepted December 15, 2012)

Abstract. For shield TBM (Tunnel Boring Machine) tunnel lining, the segment joint is the most critical component for determining the mechanical response of the complete lining ring. To investigate the mechanical behavior of the segment joint in a water conveyance tunnel, which is different from the vehicle tunnel because of the external loads and the high internal water pressure during the tunnel's service life, full-scale joint tests were conducted. The main advantage of the joint tests over previous ones was the definiteness of the loads applied to the joints using a unique testing facility and the acquisition of the mechanical behavior of actual joints. Furthermore, based on the test results and the theoretical analysis, a mechanical model of segment joints has been proposed, which consists of all important influencing factors, including the elastic-plastic behavior of concrete, the pre-tightening force of the bolts and the deformations of all joint components, i.e., concrete blocks, bolts and cast iron panels. Finally, the proposed mechanical model of segment joints has been verified by the aforementioned full-scale joint tests.

Keywords: shield TBM tunnel; segment joint; full-scale; mechanical model; joint test

1. Introduction

Due to the evolution of construction techniques and the development of tunnel boring machines (TBM), the shield-driven tunneling method has been widely adopted for the construction of metro tunnels, road tunnels and water conveyance tunnels under different conditions, such as thin soil coverage and high ground and water pressures. In shield TBM tunnels, segmental linings connected by bolts are generally employed to facilitate the erection of a complete lining ring and the reduction of the construction time. Given the complex structure of segmental lings, structural response of these linings should be investigated carefully to optimize its design and obtain the maximum safety at minimum cost.

In engineering practice, experimental tests and numerical simulations are often conducted to investigate the structural response of tunnel linings, including complete-ring tests (Munfahna *et al*. 1992, Asakura *et al*. 1992, Wang *et al*. 2001, Nakamura *et al*. 2001, 2003, Blom 2002, Lu *et al*.

∗Corresponding author, Ph.D., E-mail: yanzguo@126.com
[a]Professor

2006, Molins and Arnau 2011, Yan *et al.* 2013), segment joint tests (Lu and Cui 1987, He *et al.* 2011, Yan *et al.* 2012) and 2D/3D numerical analysis (Shin 2008). In complete-ring tests, the structural response of the tunnel lining ring under different load conditions can be simulated, the structural safety of the lining ring can be evaluated, while in segment joint tests, the key parameter, i.e., the bending stiffness of segment joints, K_θ, can be obtained for analytical studies (Lee *et al.* 2001, Liao *et al*. 2008, Ding *et al*. 2004) and numerical simulations (Vervuurt *et al.* 2002, Klappers *et al.* 2006, Arnau and Molins 2011). Considering the high cost of experimental tests, a theoretical model for determining the bending stiffness of segment joints is important in the design of segmental linings. During the last decade, some models have been established to calculate the bending stiffness of segment joints (Zhang *et al*. 2000, Zhu 2006). However, few models have considered the elastic-plastic behavior of materials and the deformation of certain joint components. Furthermore, all of the above tests and analytical studies mainly focus on segment joints adopted in metro tunnels or road tunnels. However, due to the high internal water pressure, the structure of segment joints in water conveyance tunnels is different from that in other shield TBM tunnels.

In this paper, full-scale tests on the specific segment joint used in a water conveyance tunnel were conducted to investigate its mechanical behavior. Moreover, a new model for calculating the bending stiffness of this type of segment joint was proposed, which is superior to the previous mechanical model in considering the elastic-plastic behavior of concrete and the deformation of concrete and cast iron panels. Finally the validity of the proposed model was demonstrated by comparing the calculated results with the test results.

2. Full-scale joint tests

2.1 Background

The Qingcaosha water project, which will provides approximately 70% of the total water consumed in Shanghai, China, is an ambitious project involving a reservoir on the Changxing Island, two water conveyance tunnels and several booster pump stations. The water conveyance tunnels are designed as shield TBM tunnels with specific segment joint structure, which cross the Yangtze River and link the Changxing Island to the northeast part of the city. Each tunnel is 7.23 km long and is located approximately 30 m under the water table of the Yangtze River. Therefore, the tunnel structure bears significant external water and earth pressures and must also bear the internal water pressure during the service stage. The complicated load conditions and the specific segment joint structure increase the interest in studying the structural response of the tunnel linings to improve the design and the construction techniques employed for segmental tunnel linings.

2.2 Lining structure and test specimens

The lining structure of each ring consists of 6 segments (3 standard segments, *A*, 2 adjacent segments, *B*, and 1 key segment, *K*) with an external diameter of 6.8 m, a thickness of 0.48 m and a width of 1.5m, as exhibited in Fig. 1(a). The segments in the same ring are connected with 4 M36 short and straight bolts of grade 8.8 in two circumferential bolt pockets. The side closest to the adjacent segment of the circumferential bolt pocket is made of cast iron panel to satisfy the stiffness requirement of the water conveyance tunnel, as exhibited in Figs. 1(b) and 2.

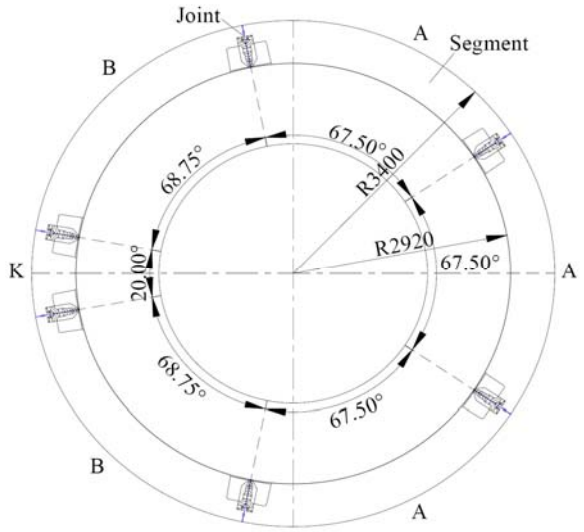

(a)

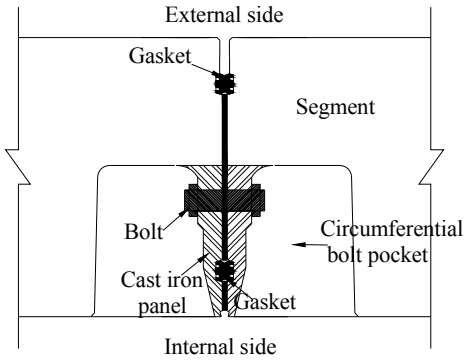

(b)

Fig. 1 The structure of the tunnel lining. (a) complete ring of the Qingcaosha tunnel lining. (b) joint structure

The reinforcement and the structural dimensions of the segments in the tests are the same as the actual segments, and they were both fabricated in the same factory to ensure that they were of identical quality. It should be noted that the circumferential dimension of the segment in the tests is a key parameter in minimizing the influence of the support on the joint's mechanical behaviors and reducing the cost of the tests. A series of FEM analyses were conducted to obtain the appropriate circumferential dimension of the segments (1/3 length of the actual segment), as exhibited in Fig. 2. The end of the segment near the support was covered with steel plates to prevent the segment from local damage during the tests.

2.3 Test set-up and programme

As exhibited in Fig. 3, the newly developed test facility consisting of self-balancing frames, hydraulic jacks, steel supports and an operation system and is approximately 4000 mm wide, 3000

mm high and 3000 mm thick. A series of tests on the mechanical response of shield TBM tunnel linings, such as bending stiffness tests on segment joints, the shear stiffness tests on radial or circumferential joints and tests on the moment transfer coefficient between the lining rings can be conveniently conducted using this test facility by adjusting loading modes. For the bending stiffness test on segment joints, lateral and vertical hydraulic jacks were applied to simulate the axial forces and moments around the segment joints, respectively, as exhibited in Fig. 4.

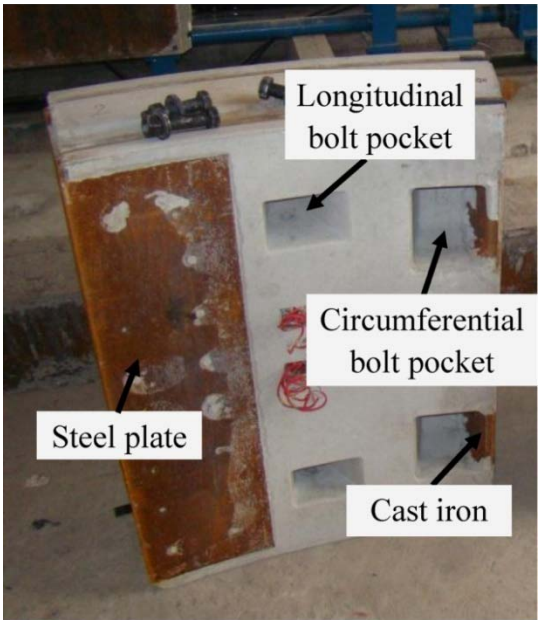

Fig. 2 Specimens employed in the full-scale joint tests

Fig. 3 Newly developed testing facility for full-scale joint tests

As exhibited in Fig. 5, the joint openings were measured by displacement sensors (V1-V4) instrumented on the segment external and internal side, respectively. The axial strain of the bolts was measured by strain gauges (HT1 and HT2), which were embedded into a hole drilled at the center of the bolts. As exhibited in Fig. 6, the circumferential concrete strain near the external side and internal side around the joint were measured by six strain gauges (Z1-Z6), respectively.

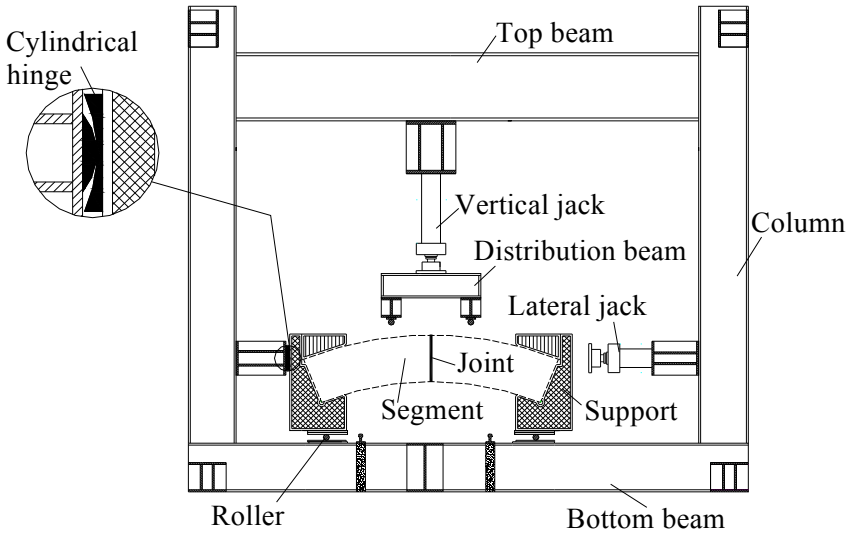

Fig. 4 Schematic of the bending stiffness test on segment joints

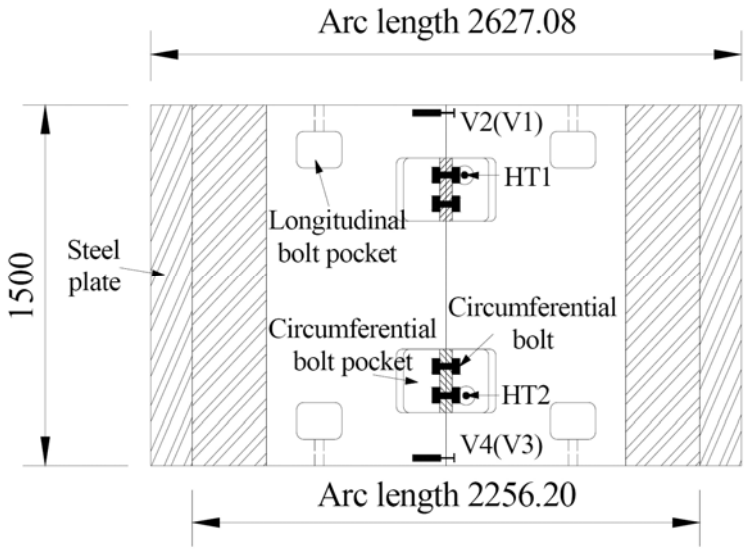

Fig. 5 Schematic diagram of the displacement sensors and bolt strain gauges (unit: mm)

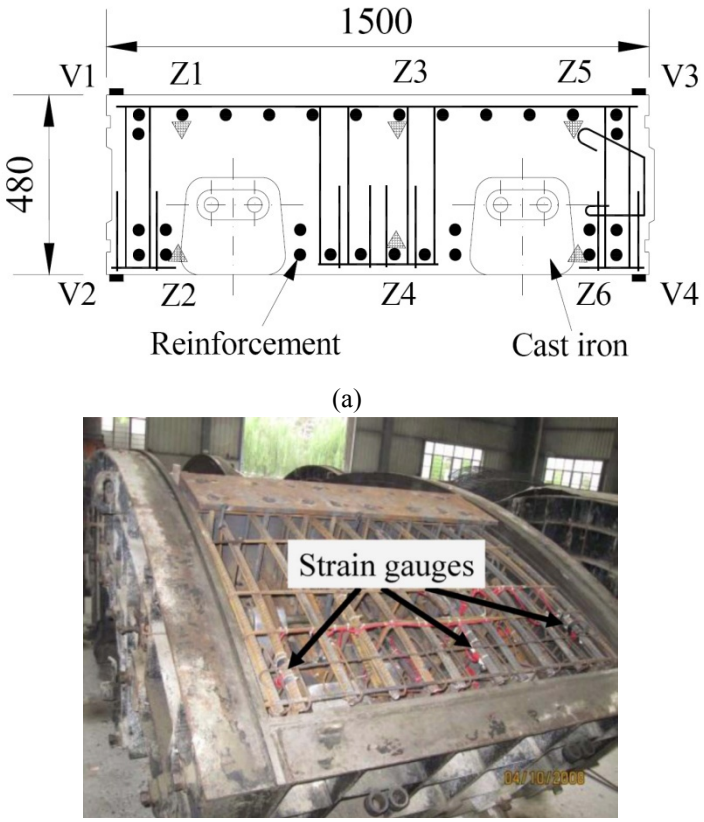

Fig. 6 Schematic diagram of circumferential concrete strain gauges in the segment. (a) Gauge arrangement (b) Gauge position in the segment

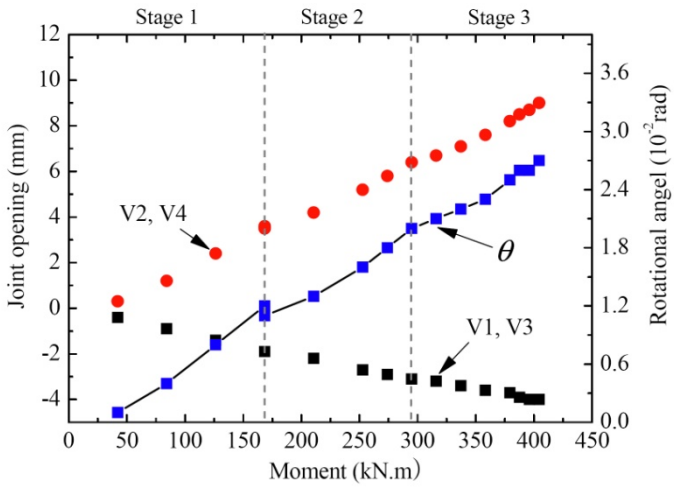

Fig. 7 Variation of joint opening and rotational angel in various stages

To obtain the bending stiffness and structural response of the segment joints in different construction stages, three combinations of the axial forces and moments were employed in the tests, as listed in Table 1. The first combination represents the stage of segment erection (i.e., stage 1); the second combination represents the initial stage of segment bearing soil pressure (i.e., stage 2), and the third combination represents the operation stage (i.e., stage 3). Furthermore, the maximum magnitude of these loads employed in the tests was the same as that experienced under the actual work conditions of the tunnel.

Table 1 Load conditions in different stage of joint tests

	Stage 1	Stage 2	Stage 3
N (kN)	207	362	518
M (kN·m)	0-168.5	168.5-294.9	294.9-404.5

2.4 Test results and discussions

The opening of the segment joints measured by displacement sensors (V1-V4) are presented in Fig. 7, in which the scatter labeled V2 and V4 denotes the average of measured values from the displacement sensors of V2 and V4; meanwhile, the scatter labeled V1 and V3 denotes that from the displacement sensors of V1 and V3. Considering the small opening of the joint compared with the dimension of the segment, the rotational angle can be approximately calculated by Eq. (1).

$$\theta = \frac{\delta_{V_2,V_4} - \delta_{V_1,V_3}}{h} \tag{1}$$

where δ_{v_2,v_4} and δ_{v_1,v_3} are the average of measured values from the displacement sensors of V2 and V4, and V1 and V3, respectively and h is the thickness of the segment.

As exhibited in Fig. 7, the test results indicated that there was a good linearity relationship between the rotational angle and the bending moment of the segments joint in different stages.

Figs. 8 and 9 present the circumferential strain near segment joints and bolt forces, respectively. It is observed that aforementioned concrete strains and bolt forces had a linear relationship with the bending moment of the joint. It should be noted that the relative large discreteness of values measured by strain gauges embedded in the segment may attributes to the impairment caused by concrete pouring and vibrating in the process of segment fabrication.

3. Model for calculating the bending stiffness of segment joints

3.1 Assumptions

The following assumptions are employed for proposing a model for calculating the bending stiffness of segment joints:

(1) The rotation and deformation of the segment surfaces forming the joint are very small compared with the size of the segment;

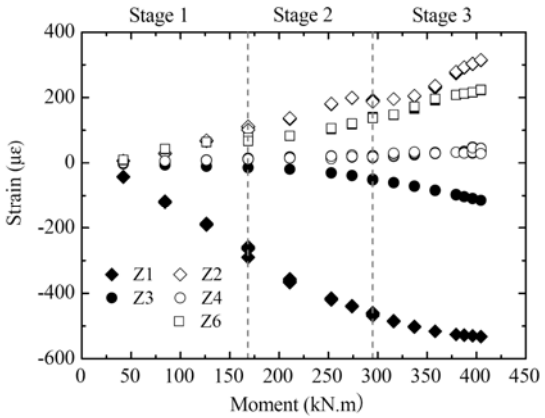

Fig. 8 Circumferential strain near the joint measured from gauges in various stages

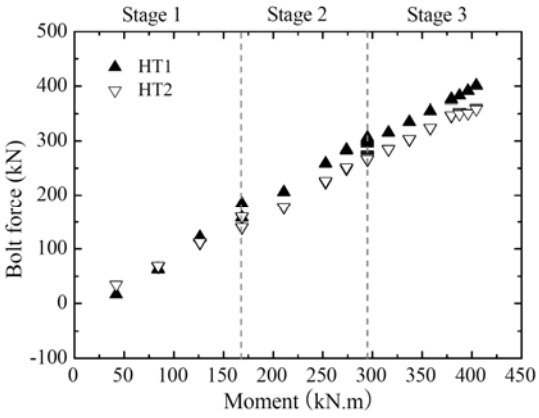

Fig. 9 Relationship between bolt forces and bending moment in various stages

(2) To calculate the rotational angle of the joint, its surface is a plane before and after bending;

(3) At a joint, the bolt is assumed to bear a tension force, and the concrete block only resists the compression force;

(4) The stiffness of the gasket (sealing rubber) is ignored because the force in the gasket is small compared with that in the concrete.

3.2 Stress-strain relationships of materials

(1) Segment concrete

According to the code for the design of concrete structures in China (GB50010-2002), the stress-strain relationship of segment concrete is expressed by

$$\left.\begin{aligned} \sigma_{\mathrm{c}} &= f_{\mathrm{c}}\left[1-\left(1-\frac{\varepsilon_{\mathrm{c}}}{\varepsilon_0}\right)^2\right] \quad (\varepsilon_{\mathrm{c}} \le \varepsilon_0) \\ \sigma_{\mathrm{c}} &= f_{\mathrm{c}} \qquad\qquad\qquad\quad (\varepsilon_0 \le \varepsilon_{\mathrm{c}} \le \varepsilon_{\mathrm{cu}}) \end{aligned}\right\} \tag{2}$$

where σ_c is stress in concrete; f_c is compressive strength of concrete; ε_c is strain in concrete; ε_0 is strain when σ_c reaches f_c and ε_{cu} is the maximum compressive strain in concrete.

(2) Bolt

The bolts used to connect the segments are considered to be an ideal elastic-plastic material, and its tension force can be calculated by

$$\left.\begin{aligned} \sigma_{\mathrm{b}} &= \sigma_0 + E_{\mathrm{b}}\varepsilon_{\mathrm{b}} \quad (\sigma_{\mathrm{b}} < f_{\mathrm{b}}) \\ \sigma_{\mathrm{b}} &= f_{\mathrm{b}} \qquad\quad (\sigma_{\mathrm{b}} \ge f_{\mathrm{b}}) \end{aligned}\right\} \tag{3}$$

where σ_b is stress in the bolt; σ_0 is pre-stress in the bolt; E_b is elastic modulus; ε_b is strain in the bolt and f_b is yield stress of the bolt.

3.3 Mechanical model of the segment joint

The detailed structure of the joint is exhibited in Fig. 10. A mechanical model of the joint is established according to the guidelines for designing the shield tunnel lining (ITA 2000), in which the bolts are treated as reinforcement and the forces in the gasket are ignored.

Based on the strain distribution in Fig. 10, the following equation can be obtained

$$\frac{\varepsilon_b}{\varepsilon_c} = \frac{h_2 - X_n}{X_n} \tag{4}$$

where ε_c is the maximum compression strain in the concrete block; ε_b is the tension strain in the bolt; h_2 is the distance between the gasket and the center of the bolt and X_n is the distance between the gasket and the neutral axis.

According to force and moment equilibrium conditions at the joint, we can obtain

$$N = F_c - T \tag{5}$$

$$M = T(h_b - \frac{h}{2}) + F_c(h_2 - h_b + \frac{h}{2} - y_c) \tag{6}$$

The meanings of h_2, h and h_b are indicated in Fig. 10. The force in the bolt, T, can be calculated by Eq. (7). In Eq. (7), T_0 is the pre-tightening force in the bolt (refer to Eq. (3)). Furthermore, based on the force and moment equivalent principle in the concrete compression zone of the segment joint (refer to Fig. 10), F_c and y_c can be determined according to the value of ε_c: a) $\varepsilon_c < \varepsilon_0$, the first expression of σ_c is employed (refer to Eq. (2)), and F_c and y_c can be calculated by Eq. (8); b) $\varepsilon_0 \leq \varepsilon_c \leq \varepsilon_{cu}$, the second expression of σ_c is employed, and F_c and y_c can be determined by Eq. (9).

$$\left.\begin{aligned} T &= T_0 + A_\mathrm{b} E_\mathrm{b} \varepsilon_\mathrm{b} \quad (\sigma_\mathrm{b} < f_\mathrm{b}) \\ T &= A_\mathrm{b} f_\mathrm{b} \qquad\qquad (\sigma_\mathrm{b} \geq f_\mathrm{b}) \end{aligned}\right\} \tag{7}$$

$$\left.\begin{aligned} F_\mathrm{c} &= f_\mathrm{c} B X_\mathrm{n} \left(\frac{\varepsilon_\mathrm{c}}{\varepsilon_0} - \frac{\varepsilon_\mathrm{c}^2}{3\varepsilon_0^2} \right) \\ y_\mathrm{c} &= \frac{X_\mathrm{n}\left(\frac{1}{3} - \frac{\varepsilon_\mathrm{c}}{12\varepsilon_0} \right)}{1 - \frac{\varepsilon_\mathrm{c}}{3\varepsilon_0}} \end{aligned}\right\} \tag{8}$$

$$\left.\begin{aligned} F_\mathrm{c} &= f_\mathrm{c} B X_\mathrm{n} \left(1 - \frac{\varepsilon_0}{3\varepsilon_\mathrm{c}} \right) \\ y_\mathrm{c} &= X_\mathrm{n} \left[1 - \frac{\frac{1}{2} - \frac{1}{12}\left(\frac{\varepsilon_0}{\varepsilon_\mathrm{c}} \right)^2}{1 - \frac{\varepsilon_0}{3\varepsilon_\mathrm{c}}} \right] \end{aligned}\right\} \tag{9}$$

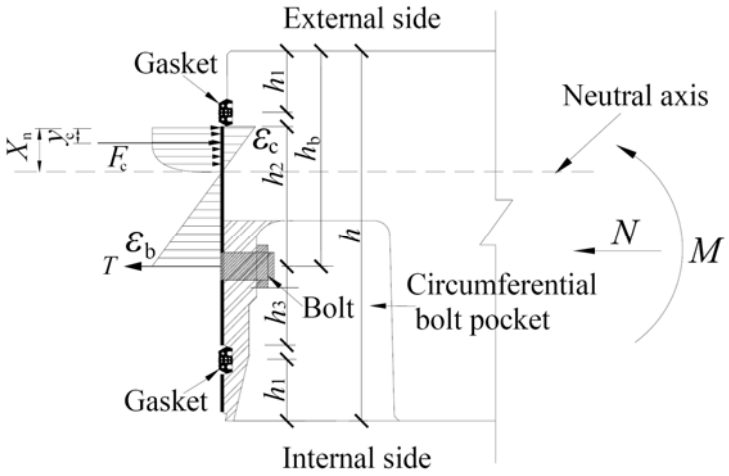

Fig. 10 Balance of force in the joint area

where B is the width of a segment. In the above equations, the basic variables are X_n, ε_n and ε_b, which can be solved by Eqs. (4)-(6). However, y_c, F_c and T in Eqs. (5) and (6) are functions of X_n, ε_c and ε_b as present in Eqs. (7)-(9). Therefore, to find a solution, iterations are needed.

3.4 Deformation model of the segment joint

Under the positive bending moment and axial force, the concrete segment will have a flexural deformation similar to that of a simple beam. As exhibited in Fig. 11(a), near the external side of the segment, a compression zone forms, and while at near the internal side, there is an opening zone.

Fig. 11(b) exhibited the deformation model of the segment joint. Δ_c is the deformation of the compression zone, and it will be discussed in Section 3.5; Δ_b is the deformation of the bolt, $\Delta_b = l_b \varepsilon_b$; δ_1 is the deformation at the external side of a segment, which can be determined by Δ_c and Δ_b according to the plane-surface assumption (refer to Section 3.1); and δ_c is the deformation at the internal side of a segment at the midline of the cast iron panel;

Fig. 12(a) shows the deformation of the cast iron panel during the full-scale joint tests. Due to the constraint effect of the bolt, the deformation around the midline of the cast iron panel is relatively small and approximately equal to that of the bolt. Toward the internal side of the joint, the deformation linearly increases with the distance from the middle line.

Fig. 12(b) represents the deformation model of the area around the bolt pocket. Based on the assumption about δ_2 (see Fig. 12) and the symmetry of the segments, the deformations of joint at the internal side can be calculated as

$$\delta_2 = \delta_c + 2w_{max}\frac{c_h}{b_h} \tag{10}$$

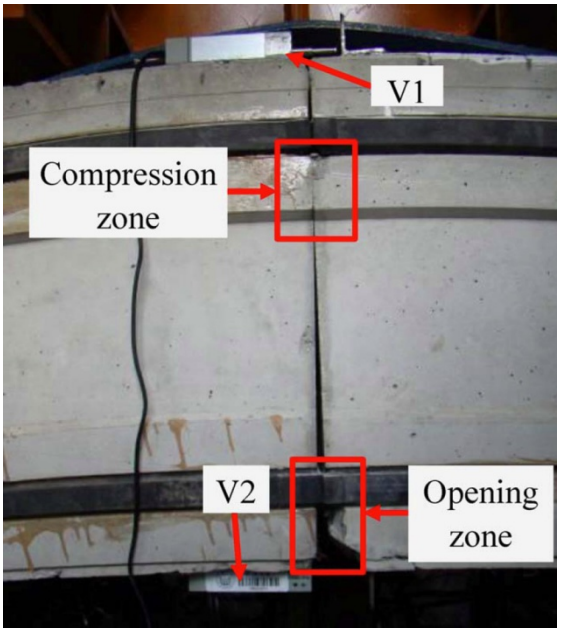

(a)

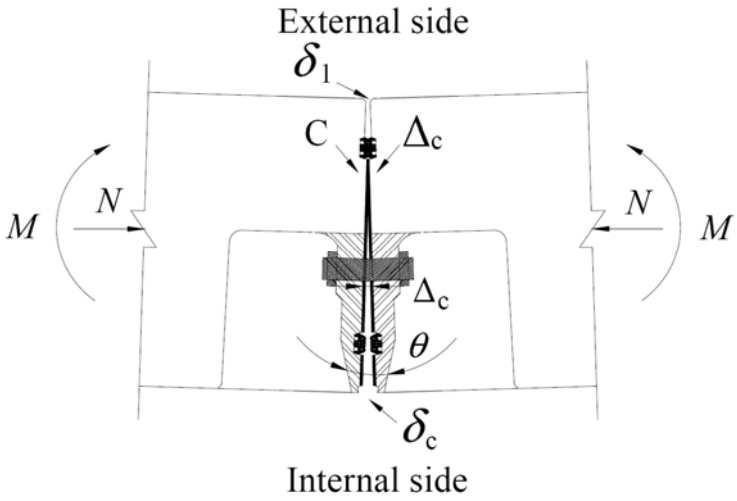

(b)

Fig. 11 Side view of the deformation pattern of the segment. (a) Side view of segments being tested. (b) Side view of the schematic diagram of the deformation

where w_{max} is the maximum deformation of the cast iron panel with the tensile force in the bolts; c_h is the distance between the center of the cast iron panel and the internal side of the segment.

Then, the rotational angle, θ, of the joint can be calculated by

$$\theta = \arctan \frac{\delta_1 + \delta_2}{h} \tag{11}$$

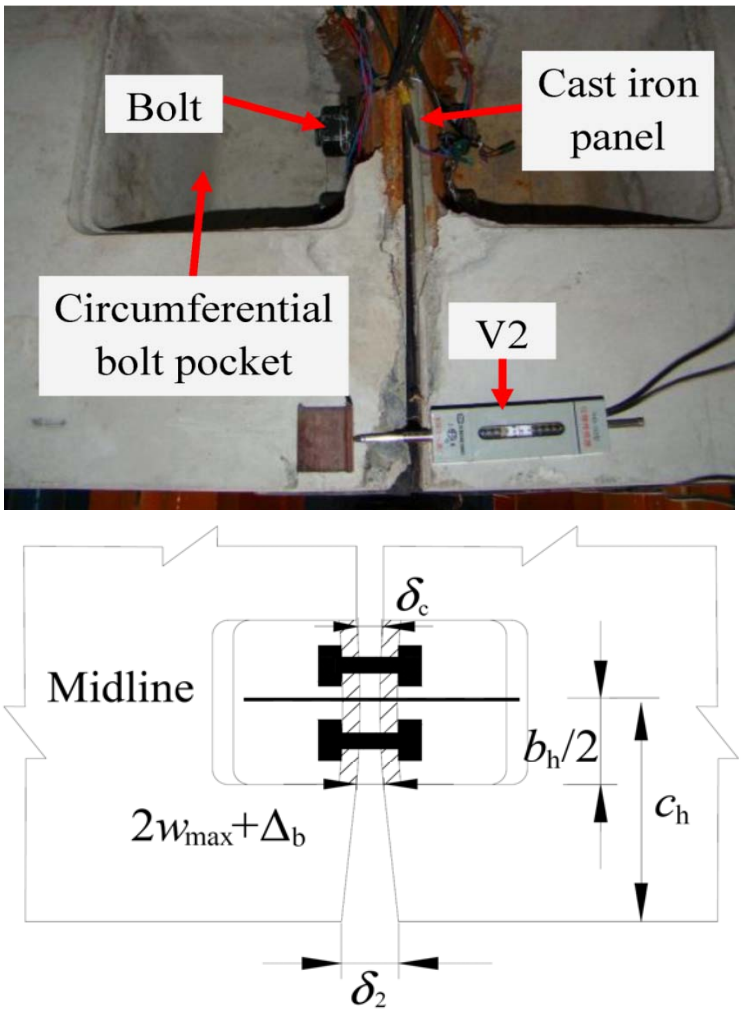

Fig. 12 Deformation pattern of the segment from the internal side. (a) segment in tests viewed from the internal side. (b) schematic diagram of deformation from the internal side

3.5 Evaluation of key parameters Δ_c and w_{max}

In this paper, the deformation, Δ_c, of the compression zone is determined by the strain on the surface of the compression zone, ε_c, and the length of the disturbed region, l_{cc}. Then, Δ_c at point C (see Fig. 11(b)) is

$$\Delta_c = 2l_{cc}\varepsilon_c \tag{12}$$

The way to evaluate ε_c is given in Section 3.3, and the way to evaluate l_{cc} is described below.

When a compressive force is applied to a small area of the joint surface, a compression zone is formed, in which the compression stress changes significantly, as exhibited in Fig. 13. The closer

to the load point, the more complex the distribution of the stresses is. From the Fig. 13, it can be observed that the circumferential stress, σ_z, is the largest at the joint surface. After a certain distance from the load point, it becomes uniform and uniaxial, i.e., $\sigma_z = F_c / (Bh)$ and $\sigma_y = 0$. According to Saint-Venant's principle, the disturbed region extends over a length approximately the thickness of the segment h (Collins and Mitchell 1991). In this study, the value of l_{cc} is investigated based on finite element analysis (FEA). From FEA, Δ_c can be obtained. Then, with the known value of σ_c, l_{cc} can be calculated from Eq. (12). In the FEA, the concrete segment is considered to be an elastic-plastic material, and the properties adopted are listed in Table 2.

A series of FEAs were conducted, and the numerical results indicated that the values of l_{cc} were mainly influenced by h, h_1 and X_n. Therefore, three dimensionless quantities are defined: $\eta = l_{cc}/ h$, $\zeta = h_1 / h$ and $\xi = X_n / h$. The relationships between η, ζ and ξ are exhibited in Fig. 14. Based on Fig. 14, the value of l_{cc} can be determined according to the values of h, h_1 and X_n.

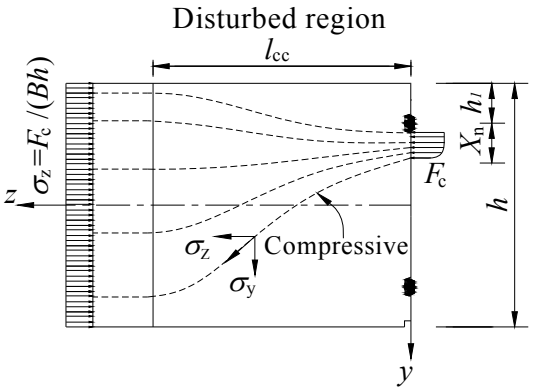

Fig. 13 Principal stress trajectories in the disturbed region

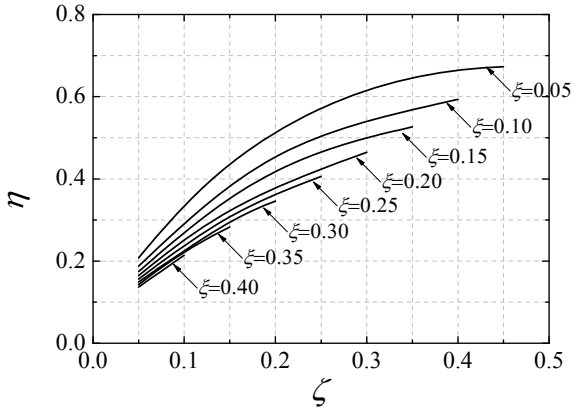

Fig. 14 Relationship between η, ζ and ξ

Table 2 Material properties adopted in FEA

Material	Elastic module (MPa)	Poisson's ratio	Yield stress (MPa)
Concrete (C55)	3.55×10^4	0.167	25.3

Table 3 Calculation parameters of the segment block

Item	Value
B (mm)	1497
h (mm)	480
h_2 (mm)	184
h_b (mm)	280
h_c (mm)	142
f_c (MPa)	25.3

Furthermore, given the cast iron panel is thin, it is simplified as a square plate ABCD with sides a_h and b_h and a uniform thickness h_h, as exhibited in Fig. 15. It is simply supported along AB, BC and AD, but free along CD. A uniform load, q, is applied to the entire surface. The plate has an isotropic bending stiffness of D. Along the boundary line CD, the maximum displacement occurs at the midpoint of CD, which can be calculated by the following formula (Johnson 1986)

$$w_{\max} = \eta_{\mathrm{p}} \frac{q h_{\mathrm{h}}^4}{D} \tag{13}$$

where q is the uniform load, $q = T/a_h b_h$; D is bending stiffness of the cast iron panel, $D = E_h h_h^3 / 12(1-v^2)$; h_h is the average thickness of the cast iron panel; v is Poisson's ratio for cast iron; a value of 0.3 is adopted and η_p is a coefficient of 0.01285 according to the Handbook of Building Structural Statistics (1998).

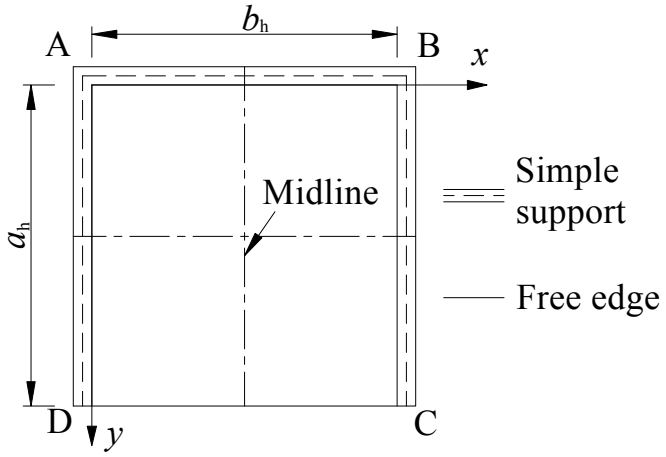

Fig. 15 Simplified edges of a cast iron panel

3.6 Procedure for calculating the bending stiffness

The procedure for calculating the bending stiffness, K_θ, can be summarized as follows:
(1) Solve ε_c and ε_b using Eqs. (3), (4), (5), (6) and (7);
(2) Calculate Δ_c from Eq. (12) and $\Delta_b = l_b \varepsilon_b$;
(3) Calculate $w_{\max}$, δ_3 and θ from Eqs. (10), (11) and (13);
(4) Calculate K_θ.

4. Comparison between the tests and the calculation results

4.1 Parameters adopted for the calculation

In this section, the actual applied member forces were used in the equations to calculate the tension force in the bolts and the deformations of the segment joint. The parameters adopted in the proposed segment joint model are listed in Tables 3-5. The calculated values are compared with the test results. Given that the maximum loads employed in the tests and the theoretical model are equal to the designed loads of the Qingcaosha tunnel in operation stage, the mechanical response of the segment joints is mainly in elastic range (refer to Figs. 16-18).

Table 4 Calculation parameters of the bolt

Item	Value
A_b (mm^2)	4069.4
l_b (mm)	114
f_b (MPa)	640
E_b (MPa)	2.1×10^5
T_0 (kN)	133.2

Table 5 Calculation parameters of the cast iron panel

Item	Value
E_b (MPa)	2.0×10^5
a_h (mm)	260
b_h (mm)	260
h_h (mm)	32.7
c_h (MPa)	480

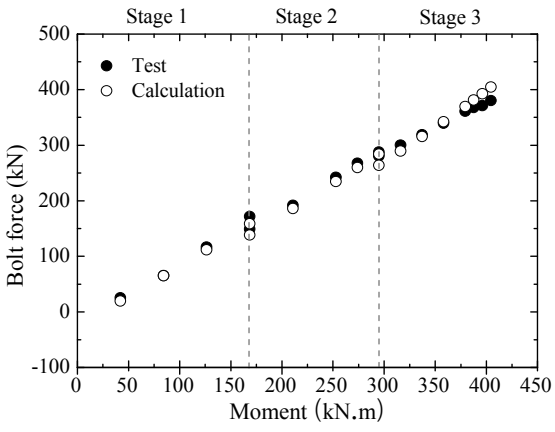

Fig. 16 Relationship between the tension force in bolts and the moment of the test and calculation values

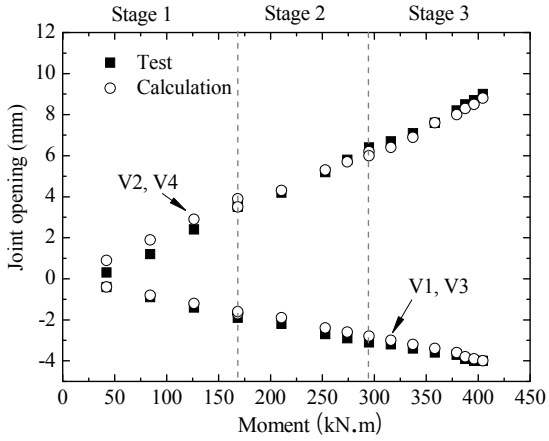

Fig. 17 Relationship between the joint openings and the moment of the test and calculation values

4.2 Tension force in the bolt

A comparison between the calculated values and the test results of the tension force in the bolt is shown in Fig. 16. It can be observed that the calculated values agree well with the test results. The maximum error is approximately 7%.

4.3 Joint openings

In Fig. 17, the calculated joint openings, δ_1 and δ_2, are compared with the test values. It can be observed that there is good agreement between them.

4.4 Rotational angle and bending stiffness of the joint

Fig. 18 presents the calculated values and the test results of the rotational angle. By comparison, it is proven that they are consistent and agree well. The maximum error is approximately 9%. Furthermore, as observed in Fig. 18, the bending moment is in proportion to the rotational angle of the joint, when the axial load is keeping constant. The bending stiffness, obtained from the tests and calculations are listed in Table 6. It can be observed that the calculated values agree well with the test results.

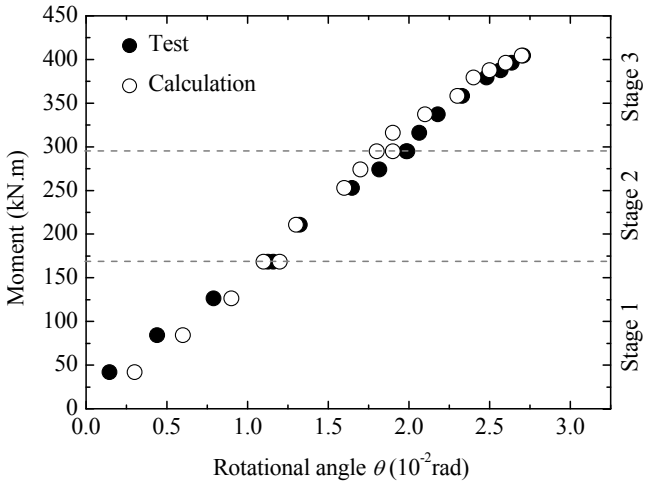

Fig. 18 Relationship between the rotational angle and the moment of the test and calculation values

Table 6 Comparison between the bending stiffness (K_θ) of segment joints obtained with the proposed model and those obtained experimentally

N (kN)	Test (kN·m/rad)	Calculation (kN·m/rad)
207	12400	14000
362	14300	13700
518	14600	12100

5. Conclusions

Full-scale joint tests were carried out to investigate the mechanical behavior of the segment joint in a water conveyance tunnel. Furthermore, a mechanical model of segment joints has been proposed. Based on the tests and analytical results, the following conclusions can be drawn.

(1) In total, eight full-scale joint tests were conducted under the field conditions of the Qingcaosha water tunnel in Shanghai. The test results revealed that (a) the opening of the joint linearly increased from the center of the cast iron panel that is a part of the joint connection system on the internal side of the segment; (b) the relationship between bending moment and the rotational angle of the joint was linear before cracks occurred in the concrete around the cast iron panel; and (c) for the conditions tested, the weaker part of the joint connection system was the concrete around the cast iron panel.

(2) Based on the test results and the theoretical analysis, a new mechanical model for calculating the bending stiffness of the segment joint has been proposed. The method considers all the important influencing factors, especially the deformation of the cast iron panel which was ignored by other methods.

(3) The proposed mechanical model was applied to the conditions of the full-scale joint tests. Comparing the calculated and the measured bending stiffness indicates that the agreement between them is quite good. It is suggested that the proposed model can be used for designing the tunnel lining systems with structures similar to those investigated in this study.

Acknowledgments

This research work is sponsored by the National Natural Science Foundation of China (50878149), the National Basic Research Program of China (973 Program:2011CB013800), the Kwang-Hua Fund for the College of Civil Engineering of Tongji University, the Fundamental Research Funds for the Central Universities and the Program for Changjiang Scholars and Innovative Research Team in University (PCSIRT,IRT1029).

The authors would also like to express their gratitude to Prof. J.C. Chai at Saga University, Japan. During his stay at Tongji University as a Kwang-hua Lecture Professor, he made several constructive suggestions for revising/modifying this paper. Shanghai Qingcaosha Investment Construction Development Co., Ltd, Shanghai Municipal Engineering Design General Institute, and Shanghai Tunnel Engineering & Rail Transit Design and Research Institute are also acknowledged for helping conduct the full-scale joint tests.

References

Arnau, O. and Molins, C. (2011), "Experimental and analytical study of the structural response of segmental tunnel linings based on an in situ loading test, Part 2: Numerical simulation", *Tunnelling and Underground Space Technology*, **26**(6), 778-788.

Asakura, T., Kojima, Y., Ando, T. and SATO, Y. (1992), "Analysis of the behavior of tunnel lining - experiment and simulation on double track tunnel lining", *Quarterly Reports of Railway Technical Research Institute in Japan*, **33**(4), 266-273.

Blom, C.B.M. (2002), "Design Philosophy of Concrete Linings for Tunnels in Soft Soils", Ph. D. Thesis, Technische Universiteit Delft, Delft, Netherlands.

Collins, M.P. and Mitchell, D. (1991), *Prestressed Concrete Structures*, Prentice Hall, Englewood Cliffs, New Jersey.

Ding, W.Q., Yue, Q.Z., Tham, G.L., Zhu, H.H., Lee, C.F. and Hashimoto, T. (2004), "Analysis of shield tunnel", *International Journal for Numerical and Analytical Methods in Geomechanics*, **58**, 57-91.

He, C., Feng, K. and Su, Z.X. (2011), "Development and application of loading test system of prototype structure for underwater shield tunnel with large cross-section", *Chinese Journal of Rock Mechanics and Engineering*, **30**(2), 254-266.

Johnson, D. (2000), *Advanced Structural Mechanics*, Thomas Telford Limited, London.

Klappers, C., Grübl, F. and Ostermeier, B. (2006), "Structural analyses of segmental lining - coupled beam and spring analyses versus 3D-FEM calculations with shell elements", *Proceedings of the ITA-AITES 2006 World Tunnel Congress*, Seoul, April.

Lee, K.M., Hou, X.Y., Ge, X.W. and Tang, Y. (2001), "An analytical solution for a jointed shield-driven tunnel lining", *International Journal for Numerical and Analytical Methods in Geomechanics*, **25**, 365-390.

Liao, S.M., Peng, F.L. and Shen, S.L. (2008), "Analysis of shearing effect on a tunnel induced by load transfer along longitudinal direction", *Tunnelling and Underground Space Technology*, **23**, 421-430.

Lu, L., Lu, X. and Fan, P. (2006), "Full-ring experimental study of the lining structure of Shanghai changing tunnel", *Proceedings of the 4th International Conference on Earthquake Engineering*, Taiwan, October.

Lu, T.S. and Cui, T.J. (1987), "Test and Research on Lining Radial Joint Stiffness", *Underground Engineering and Tunnels*, **8**(4), 21-25.

Ministry of Construction P.R. China (2002), Code for design of concrete structures (GB50010-2002), China Architecture & Building Press, Beijing.

Molins, C. and Arnau, O. (2011), "Experimental and analytical study of the structural response of segmental tunnel linings based on an in situ loading test. Part 1: Test Configuration and Execution", *Tunnelling and Underground Space Technology*, **26**(6), 764-777.

Munfahna, Michaelp, Dellap (1992), "Full scale testing of tunnel liner", *Proceedings of the International Congress 'Towards New Worlds in Tunnelling'*, Acapulco, May.

Nakamura, H., Nakagawa, Y., Okamoto, N., Mizita, S. and Nakao, T. (2001), "Utilization examination of a shield driven tunnel of large rectangular shape", *Proceedings of Tunnel Engineering, JSCE*, **11**, 351-356.

Nakamura, H., Kubota, T., Furukawa, M. and Nakao, T. (2003), "Unified construction of running track tunnel and crossover tunnel for subway by rectangular shape double track cross-section shield machine", *Tunneling and Underground Space Technology*, **18**(2), 253-262.

Shin, J.H. (2008), "Numerical modeling of coupled structural and hydraulic interactions in tunnel linings", *Structural Engineering and Mechanics*, **29**(1), 1-16.

Vervuurt, A.H.J.M., Van der Veen, C., Gijsbers, F.B.J. and den Uijl, J.A. (2002), "Numerical simulations of tests on a segmented tunnel lining", *Procedings of the 3rd DIANA World Conference*, Tokyo, October.

Wang, R.L., Song, B., Wang, Q. and Zheng, B. (2001), "Lining experiment and structure analysis of bi-circular shield tunnel with staggered joint splice on segments", *Underground Engineering and Tunnels*, **1**, 12-15.

Working Group No. 2, International Tunneling Association (ITA) (2000), "Guidelines for the Design of Shield Tunnel lining", *Tunnelling and Underground Space Technology*, **15**(3), 303-331.

Working group of Handbook of Building Structural Statics (1998), *Handbook of Building Structural Statics* (Second Edition), China Architecture & Building Press, Beijing.

Yan, Z.G., Zhu, H.H., Ju, J.W. and Ding W.Q. (2012), "Full-scale fire tests of RC metro shield TBM tunnel linings", *Construction and Building Materials*, **36**, 484-494.

Yan, Z.G., Zhu, H.H. and Ju, J.W. (2013), "Behavior of reinforced concrete and steel fiber reinforced concrete shield TBM tunnel linings exposed to high temperatures", *Construction and Building Materials*, **38**, 610-618.

Zhang, H.M., Guo, C. and Fu, D.M. (2000), "A study on the stiffness model of circular tunnel prefabricated lining", *Chinese Journal of Geotechnical Engineering*, **22**(3), 309-313.

Zhu, W., Zhong, X.C. and Qin, J.S. (2006), "Mechanical analysis of segment joint of shield tunnel and research on bilinear joint stiffness model", *Rock and Soil Mechanics*, **27**(12), 2154-2158.